Chemotherapeutic Delivery from a Self-Assembling Peptide Nanofiber Hydrogel for the Management of Glioblastoma

Citation: Pharmaceutical Research. 2018 Jun 25;35(8):166

As Published: https://doi.org/10.1007/s11095-018-2442-1

Publisher: Springer US

Persistent URL: https://hdl.handle.net/1721.1/131496

Version: Author's final manuscript: final author's manuscript post peer review, without publisher's formatting or copy editing

Chemotherapeutic delivery from a self-assembling peptide nanofiber hydrogel for the management of glioblastoma

Christina Karavasili,[1] Emmanuel Panteris,[2] Ioannis S. Vizirianakis,[3] Sotirios Koutsopoulos,[4] Dimitrios G. Fatouros [1,]*

[1]School of Pharmacy, Aristotle University of Thessaloniki, Department of Pharmaceutical Technology, GR-54124 Thessaloniki, Greece

[2]Department of Botany, School of Biology, Aristotle University of Thessaloniki, GR-54124 Thessaloniki, Greece

[3]School of Pharmacy, Aristotle University of Thessaloniki, Laboratory of Pharmacology, GR-54124 Thessaloniki, Greece

[4]Center for Biomedical Engineering, Massachusetts Institute of Technology, 77 Massachusetts Avenue, Cambridge, MA 02139, USA

Abstract

Purpose: Localized chemotherapy has gained significant impetus for the management of malignant brain tumors. In the present study, we appraised the versatility of an *in-situ* gel forming self-assembling peptide, ac-$(RADA)_4$-$CONH_2$, as a biocompatible delivery depot of the chemotherapeutic drug doxorubicin (DOX) and the anticancer agent curcumin (CUR), respectively.

Methods: The morphology and mechanical properties of ac-$(RADA)_4$-$CONH_2$ were assessed with scanning electron microscopy (SEM) and rheological studies. The *in vitro* drug release from ac-$(RADA)_4$-$CONH_2$ was monitored in phosphate-buffered saline pH 7.4. Distribution of the fluorescent actives within the peptide matrix was visualized with confocal laser scanning microscopy (CLSM) The *in vitro* biological performance of the ac-$(RADA)_4$-$CONH_2$-DOX and ac-$(RADA)_4$-$CONH_2$-CUR was evaluated on the human glioblastoma U-87 MG cell line.

Results: SEM studies revealed that the ac-$(RADA)_4$-$CONH_2$ hydrogel contains an entangled nanofiber network. Rheology studies showed that the more hydrophobic CUR resulted in a stiffer hydrogel compared with ac-$(RADA)_4$-$CONH_2$ and ac-$(RADA)_4$-$CONH_2$-DOX, due to the interaction of CUR with the hydrophobic domains of the peptide nanofibers as confirmed by CLSM. *In vitro* release studies showed a complete DOX release from ac-$(RADA)_4$-$CONH_2$ within 4 days and a prolonged release for ac-$(RADA)_4$-$CONH_2$-CUR over 20 days. An increased cellular uptake and a higher cytotoxic effect were observed for ac-$(RADA)_4$-$CONH_2$-DOX, compared with DOX solution. Higher levels of early apoptosis were observed for the cells treated with the ac-$(RADA)_4$-$CONH_2$-CUR, compared to CUR solution.

Conclusions: The current findings highlight the potential utility of the in-situ depot forming ac-$(RADA)_4$-$CONH_2$ hydrogel for the local delivery of both water-soluble and insoluble chemotherapeutic drugs.

Keywords: self-assembly, drug delivery, cancer treatment, doxorubicin, curcumin

Abbreviations

CUR	Curcumin
DOX	Doxorubicin
SEM	Scanning electron microscopy
GBM	Glioblastoma multiforme
BBB	Blood brain barrier
CLSM	Confocal laser scanning microscopy
PBS	Phosphate-buffered saline
IC_{50}	Half-maximal inhibitory concentration

Introduction

Glioblastoma multiforme (GBM) constitutes a highly malignant primary brain tumor arising from glial cells. Although GBM had a relatively low reported incidence rate of 3 cases per 100,000 people in the United States and Europe, increased attention has been drawn into the development of new treatment approaches because of its poor prognosis with a median survival rate of 15 months (1). Standard treatment options comprise surgical resection, where possible, with adjuvant chemotherapy and/or radiation (2,3). However, current treatments and prognosis are highly dependent on the circumstantial glioma features including the tumor's anatomic topographic location that impedes radical resection, high tumor heterogeneity, cell infiltration to adjacent brain tissue and inherent resistance to chemotherapy (4). Also, the presence of the brain's natural barrier [i.e., Blood brain barrier (BBB), enzymatic barrier, efflux transporter system] poses a significant obstacle to the delivery of therapeutic concentrations of cytotoxic drugs at the tumor site (5). Therefore, even after following the mainstay of therapeutic options, prolonged remission is not guaranteed, resulting in a poor outcome in GBM patients with tumor recurrence and a life expectancy only extended by 3 months to 1 year (6).

The development and adoption of efficacious therapeutic approaches after first line therapy failure, comprises of GBM patient introduction in clinical trial protocols including gene and vaccine therapy, immunotherapy (7) and localized drug delivery strategies (8). Local implantable or injectable chemotherapeutic platforms have emerged as ideal candidates to be applied in the resection cavity after surgery, aiming to achieve high drug concentrations at the tumor site, while minimizing at the same time systemic toxicity (9). The delivery strategies deployed in the local treatment of brain cancer include implantable microdevices with drug eluting and microelectromechanical properties, nanoparticle-based delivery systems with targeting

specificity and sensitization to external stimuli such as radiation and the application of an external magnetic field, as well as injectable hydrogels (10). Currently, the only approved implantable drug for the treatment of recurrent gliomas is a biodegradable polymer loaded with carmustine (Gliadel® wafer).

Hydrogels have arisen as an attractive drug delivery platform for localized drug administration and delivery for the treatment of GBM (11). An ideal hydrogel system should convey certain physicochemical properties to fulfil the requirements of biomedical applications, with the most important being biocompatibility and biodegradability, sterility and controlled release of therapeutics for prolonged time-periods, as well as compliance with certain rheological and mechanical properties for topical administration (12). Drug encapsulation in hydrogels is achieved either through direct loading (13) or by utilizing nanosized drug delivery vectors (14), in either case characterized by high loading efficiency of both lipophilic (13) and hydrophilic (14) compounds and the ease of formulation and scale-up. A number of hydrogels has been assessed for the treatment of glioblastoma including chitosan, alginate and PLA/PLGA-based hydrogels which allow for the local delivery of chemotherapeutic drugs to the brain (1). Recent advances in the field of injectable systems report on stimuli-responsive poly(ethylene glycol) 4000 hydrogels that enable enhanced tumor selectivity and drug release specificity through a matrix metalloprotease sensitive peptide linker to cis platin (15). A poly(ethylene glycol)-based hydrogel incorporating iron oxide nanoparticles demonstrated enhanced cytotoxicity with synergistic adjacent hyperthermia facilitating the delivery of both paclitaxel and heat for the treatment of cancer (16). In addition, thermoreversible poly(ethylene glycol)-g-chitosan hydrogel depots of T lymphocytes with a sol-to-gel transition occurring around ≥32 °C and a steady bioactive release were reported as a viable approach for localized immunotherapy of

glioblastoma (17), while an engineered system consisting of an intracortical tumor guide that incorporates aligned PCL nanofibers was found to significantly reduce tumor volume after implant insertion through guidance of the invasive tumor cells away from the primary tumor site to an extracortical cytotoxic cyclopamine-conjugated collagen hydrogel (18).

Hydrogel forming self-assembling peptides have also gained popularity in biomedical and drug delivery applications owing to their unique properties (19-24). They comprise of repetitive motifs of alternating ionic hydrophilic and hydrophobic natural amino acids rendering them biocompatible and biodegradable (25). Upon interaction with electrolyte solutions (either through the addition of salt solution, culture medium, or injection of the material *in vivo*), such peptides self-assemble to form highly entangled three-dimensional networks of high water content ranging from 97 % to 99.9 % w/v (19). The driving force for peptide self-assembly into stable nanofibers derives from an orchestrated combination of hydrophobic interactions, hydrogen bonding, van der Waals' interactions, and ionic interactions between the opposite charged amino acids on the hydrophilic peptide surface. Being amenable to a large array of chemical and structural interventions, one can strategically direct the molecular interactions of self-assembling peptides into supramolecular structures of well-defined and controllable functionalities. Injectable peptide hydrogels have been exploited in numerous biomedical applications in tissue engineering and regeneration (25,26).

The present study outlines the prospect of a biocompatible and bioresorbable self-assembling peptide hydrogel, ac-$(RADA)_4$-$CONH_2$, as chemotherapeutic delivery depot of doxorubicin (DOX) and curcumin (CUR) in the localized treatment of glioblastoma. The ac-$(RADA)_4$-$CONH_2$ peptide hydrogel consists of standard amino acids [CH_3CO-RADARADARADARADA-$CONH_2$, where R is arginine, A is alanine and D is aspartic acid)

with a calculated MW of 1713 Da. It comprises of alternating hydrophobic and charged residues that promote the adaptation of a *β*-strand conformation in which hydrophilic amino acids (i.e., R and D) are located on one side of the strand and hydrophobic amino acids (i.e., the A) on the other side (27). Upon self-assembly, *β*-strands arrange into an ordered nanofiber structure composed of two stacked *β*-sheets, which are stabilized by a hydrophobic core formed by alanine side chains. Doxorubicin is an antimitotic anthracycline derivative that exerts its cytotoxic action among other modes also by intercalation with the DNA double helix (28), while curcumin is a phytochemical compound that has been comprehensively evaluated for its anticancer efficacy also in the treatment of glioblastoma through modulation of cell cycle, apoptotic signals, anti-apoptotic proteins and by potentiating the efficacy of existing chemotherapeutics in combination drug therapy (29). Self-assembling peptide nanofiber ac-$(RADA)_4$-$CONH_2$ is versatile material previously used as building blocks in medical applications; as a host for small and large molecules (19, 20) or biomaterial in tissue engineering (25). To this end in this work we investigated its potentiality to serve as a carrier for chemotherapeutic agents. The *in vitro* release profiles of the chemotherapeutic actives from the self-assembling peptide hydrogel were monitored and the anti-proliferative effect and apoptotic cell response of the drug loaded hydrogel systems were evaluated in U-87 MG human glioblastoma cells. The efficacy of the hydrogel drug reservoir to enhance drug cellular accumulation was assessed both qualitatively with confocal scanning laser microscopy (CLSM) and quantitatively with flow cytometry analysis. To the best of our knowledge, this is the first application of a self-assembling peptide hydrogel for the local delivery of chemotherapeutics in the treatment of glioblastoma.

Materials and methods

Materials

Dulbecco's modified eagle's medium (DMEM), penicillin-streptomycin (10,000 U/mL), fetal bovine serum (FBS) and phosphate-buffered saline 10X (PBS) were purchased from Gibco™ (Life Technologies, Grand Island, NY, USA). 3-(4,5-dimethylthiazol-2-yl)-2,5-diphenyltetrazolium bromide (MTT) and dimethylsulfoxide (DMSO) were purchased from Sigma-Aldrich Chemie Gmbh (Munich, Germany). ProLong® Gold Antifade Mountant with DAPI was purchased from ThermoFischer Scientific (Walham, MA, USA). Triton X-100, curcumin (CUR) and doxorubicin (DOX) were purchased from Sigma-Aldrich Chemie Gmbh (Munich, Germany). Peptide aqueous solution ac-$(RADA)_4$-$CONH_2$ (1 % w/v) was obtained from PuraMatrix® (Corning, NY, USA).

Cell culture

U-87 MG human primary glioblastoma cells were cultured in DMEM supplemented with 10 % w/v FBS, 100 units/mL penicillin and 100 μg/mL streptomycin. Cells were maintained at 37 °C in a humidified atmosphere with 5 % v/v CO_2. Exponentially growing cells were used for all studies.

Methods

Scanning Electron Microscopy (SEM) studies

SEM imaging of the ac-$(RADA)_4$-$CONH_2$ peptide hydrogel was performed after slow exchange of the water in the hydrogel with ethanol in 10% v/v increment steps for 60 min in each condition. At the final step (100% ethanol), the ethanol was replaced with liquid CO_2 using a CO_2 critical point dryer (Balzers CPD 030). Once the substitution was complete, the samples

were carefully affixed onto 12.5 mm SEM stubs and coated with ~3 nm of Platinum (Quorum Q150T ES) and the nanofiber framework was visualized by SEM (FEI Quanta FEG 250 Scanning Electron Microscope, FEI Co., Hillsboro, Oregon, USA).

Preparation of the drug loaded ac-$(RADA)_4$-$CONH_2$ peptide hydrogel

For the preparation of the ac-$(RADA)_4$-$CONH_2$-DOX, the drug was dissolved in the aqueous peptide solution (1% w/v) at a final concentration of 5 mg/mL. For CUR loading in the ac-$(RADA)_4$-$CONH_2$ peptide hydrogel, two microliters of drug's ethanolic solution (5 mg/mL) were introduced in the peptide solution (1 % w/v) at a final drug concentration of 222 μg/mL and sonicated till complete homogenization. In both cases, gelation occurred upon the addition of PBS solution to a final peptide concentration of 0.9 % w/v, resulting in a red or yellow colored hydrogel for ac-$(RADA)_4$-$CONH_2$-DOX and ac-$(RADA)_4$-$CONH_2$-CUR, respectively. The encapsulation efficiency of both CUR and DOX in the peptide hydrogel was 100 %.

Rheology studies

Rheology experiments were performed to determine the flow and viscoelastic behavior of the peptide nanofiber hydrogel Ac-$(RADA)_4$-$CONH_2$ prior and post drug loading on a rotational Physica MCR 300 rheometer (Physica Messtechnic GmbH, Stuttgart, Germany) using the cone and plate geometry (diameter 25 mm, cone angle 1°, at a gap of 0.05 mm). The temperature was regulated by a Paar Physica circulating bath and a controlled Peltier system (TEZ 150P/MCR) at 37 ± 0.1 ^{o}C. A vapor trap was placed around the cone to prevent liquid evaporation. Two types of rheological measurements were performed: (a) isothermal gel curing events were probed at a strain level of 0.5% and a frequency of 1 Hz and (b) oscillatory measurements of G′ (storage

modulus), G″ (loss modulus) and tan δ (G″/G′) were performed with a strain of 0.5 % and a frequency range over 0.1−100 Hz. Strain was kept intentionally low, as to remain within the linear viscoelastic regime. The data were analyzed using the rheometer software US200 V2.21. For the measurements, 600 μL of 1% w/v plain and drug loaded peptide solutions were placed on the rheometer plate and PBS pH 7.4 was added to form a peptide hydrogel of 0.9% w/v.

In vitro release studies of anticancer agents from ac-$(RADA)_4$-$CONH_2$ peptide hydrogel

In vitro drug release studies were conducted in PBS pH 7.4 at 37 ^{o}C (30,31). In the case of curcumin (CUR) release studies were performed in the presence of 0.1 % w/v Tween 80. After 30 min from the initiation of the gelation process, 1 mL of release medium was added on top of the peptide hydrogel. Samples (800 μL) were withdrawn at predetermined time-points and replaced with equal volumes of medium. Drug quantification was performed with UV-Vis analysis at 420 nm for CUR and 480 nm for DOX, respectively.

Drug release kinetics

The experimental data of CUR and DOX release from the peptide nanofiber hydrogel ac-$(RADA)_4$-$CONH_2$ were fitted to Korsmeyer-Peppas ($M_t/M_0 = K_{KP} \times t^n$) equation in order to determine drug release kinetics, where M_t/M_0 is the fraction of drug released at time t, K is the kinetic constant and n is the diffusion exponent that characterizes the release mechanism of the drug. The first 60 % drug release data were fitted to Korsmeyer-Peppas kinetic model in order to calculate the exponent of n, where $0.45 \leq n$ corresponds to a Fickian diffusion mechanism, $0.45 < n < 0.89$ to non-Fickian transport, $n = 0.89$ to Case II (relaxational) transport, and $n > 0.89$ to

super case II transport (32). Kinetic analysis of the experimental data was performed using the DDSolver program (33).

Confocal laser scanning microscopy (CLSM) studies

Localization of the fluorescent actives DOX and CUR within the ac-$(RADA)_4$-$CONH_2$ peptide hydrogel was observed by confocal microscopy. Z-stack images were acquired by step-wise scanning of the peptide hydrogel from its top to the equatorial plane at 1.16 μm steps with a 63x oil-immersion lens under a Zeiss LSM 780 CLSM (Carl Zeiss Microscopy GmbH, Berlin, Germany) with the appropriate filters. Images were acquired with ZEN 2011 software.

Determination of inhibitory drug concentrations

The half-maximal inhibitory concentrations (IC_{50}) of DOX and CUR in U-87 MG cells were determined by cell counting and were calculated as the number of viable cells divided by the total number of cells using the Trypan blue exclusion assay. The cells were plated in 24-well plates at a density of 10^5 cells / mL and were allowed to attach overnight. After 24 h the culture medium was replaced with fresh medium containing the drug solutions at the concentration range of 10^{-7} M to 10^{-4} M and cells were further cultured for 48 h. CUR was dissolved in DMSO at a final concentration of 0.2 % v/v in the culture medium. Control experiments showed that the presence of 0.2 % v/v DMSO in cell cultures had no effect on cell proliferation. The IC_{50} values were calculated from the linear regression line of the plot of percentage inhibition versus log inhibitory concentration using the sigmoidal dose response equation with variable slopes.

Cell viability assay

The effect of plain drug solutions and drug released from peptide hydrogels on the viability of U-87 MG cells was determined by the 3-(4,5-dimethylthylthiazol-2-yl)-2,5 diphenyltetrazolium bromide (MTT) assay. Cells were plated in 96-well plates at a density of $5 \cdot 10^3$ cells/well and treated with a concentration range of plain drug solutions (CUR: 1-50 μM, DOX: 0.1-10 μM), the drug loaded peptide hydrogels containing equivalent drug concentrations and the plain peptide hydrogel for 48 h. Untreated cells were used as negative control and cells treated with 1 % v/v Triton X-100 were used as positive control. After 48 h of incubation, 10 μL of MTT solution (5 mg/mL) were added to each well and the plate was further incubated for 4 h in a humidified atmosphere at 37 °C with 5 % CO_2. The supernatants were carefully discarded, and the formed formazan crystals were dissolved upon the addition of 100 μL of dimethyl sulfoxide (DMSO). After thorough mix for 15 min, the absorbance was measured using an ELISA plate reader at 570 nm. Cell viability was calculated according to equation 1:

$$\text{cell viability (\% of control)} = \frac{\text{ODtest} - \text{ODblank}}{\text{ODcontrol} - \text{ODblank}} \text{ x } 100 \quad [1]$$

Drug cellular uptake studies

Evaluation of CUR and DOX uptake by CLSM. Intracellular uptake of CUR and DOX was qualitatively assessed by CLSM. U-87 MG cells were seeded on coverslips in 6-well plates at a density of $2 \cdot 10^5$ cells/well and treated with the plain drug solutions or the drug-loaded peptide hydrogels at an equivalent to IC_{50} drug concentration (0.682 μM for DOX and 5.76 μM for CUR). After 0.5 h, 1.5 h, 3 h and 6 h of incubation, the cells were washed twice with PBS and fixed in 4% PFA solution in PBS for 15 min. The cells were then rinsed with PBS and permeabilized with 0.1 % Triton X-100 solution in PBS for 10 min. The coverslips were

mounted onto glass microscope slides in Prolong Gold Antifade Reagent with DAPI, sealed and left overnight in the dark at 4 ^{o}C. The specimens were examined with a Zeiss LSM780 CLSM, with the appropriate filters and a 40x oil-immersion lens. Images were acquired with ZEN2011 software. For comparison, the same laser intensity and gain, as well as pinhole settings were applied for all the specimens of each treatment.

Quantification of CUR and DOX uptake by flow cytometry

Intracellular uptake of CUR and DOX was quantitatively assessed using flow cytometry. U-87 MG cells were plated in 6-well plates at a density of $2 \cdot 10^5$ cells/well and treated with the plain drug solutions or the drug loaded peptide hydrogels at an equivalent to IC_{50} drug concentration. After treatment for 0.5 h, 1.5 h, 3 h and 6 h the medium was discarded, and the cells were washed with PBS, trypsinized, centrifuged (5 min, 1000 rpm) and re-suspended in PBS prior to flow cytometric analysis on a CyFlow® Cube 8 (Sysmex Partec GmbH, Goerlitz, Germany). A minimum of 15,000 cells per sample were analyzed. The fluorescence signals of CUR and DOX were collected by the FL-1 and FL-2 channels, respectively.

Apoptosis assay

Detection of cell apoptosis was performed by flow cytometry using the Annexin-V-FITC/Propidium iodide (PI) double staining method according to manufacturer's instructions (BioLegend, San Diego, CA). U-87 MG cells were plated in 6-well plates at a seeding density of $1x10^6$ cells per well and treated with the plain drug solutions or the drug loaded peptide hydrogel at an equivalent to IC_{50} drug concentration for 48 h. Untreated cells were used as the control culture. After treatment, cells were harvested, washed twice with ice-cold PBS and re-suspended

in 100 μL of Annexin-V binding buffer at a concentration of 1 x 10^6 cells/mL. Cells were stained with 5 μL Annexin-V-FITC and 10 μL PI for 15 min at room temperature in the dark, prior to flow cytometric measurements.

Statistical analysis

All data are presented as means ± standard deviation (SD). Student's t test was employed to evaluate the data. P values less than 0.05 were considered to be statistically significant.

RESULTS AND DISCUSSION

Visualization of the three-dimensional ac-$(RADA)_4$-$CONH_2$ peptide nanofiber structure

The inner three-dimensional structure of the ac-$(RADA)_4$-$CONH_2$ was examined using SEM analysis using CO_2 critical point drying to preserve the structural integrity of the peptide hydrogel. Ac-$(RADA)_4$-$CONH_2$ peptide hydrogel comprises of an interconnected nanofiber network, creating a porous matrix of nanometric alveoli (Figure 1).

Rheological properties of the drug loaded ac-$(RADA)_4$-$CONH_2$ peptide nanofiber hydrogel

The effect of CUR and DOX loading on the viscoelastic properties of the ac-$(RADA)_4$-$CONH_2$ peptide nanofiber hydrogel was investigated with rheological studies. Time sweep oscillatory measurements were conducted to monitor the mechanical strength of the plain and drug loaded peptide hydrogel during the onset of gelation (Figure 2A) over a time period of 60 minutes. All samples are gels with the storage modulus G' being about an order of size higher than the loss modulus G" throughout the timespan of the experiment. Significantly higher G' values were observed for the ac-$(RADA)_4$-$CONH_2$-CUR (i.e., 490 Pa at 23 min) compared to ac-$(RADA)_4$-

$CONH_2$ (95.4 Pa at 23 min) and ac-$(RADA)_4$-$CONH_2$-DOX (45.9 Pa at 23 min), that is at the initial stages of the gelation process. The enhancing effect of CUR on hydrogel rigidity at the initial stages of the gelation might be attributed to the hydrophobic character of CUR that facilitates the formation of an extended network of peptide nanofibers. The initial lag phase for gelation appears to end at approximately 23 min for all peptide hydrogel samples with and without encapsulated drug. Past this lag phase, the moduli increased by two orders of magnitude within 10 min, while the different hydrogels relative differences in their G´ and G´´ values was not changed.

Frequency sweep tests were conducted from 0.1 to 100 rad/sec at a constant 0.5 % strain immediately after preparation (Figure 2B). Results revealed an elastic dominant behavior of the peptide hydrogel both prior and post drug loading with storage modulus being higher than loss modulus over the entire frequency range and nearly independent of frequency. Similar G' and G'' values were obtained for the plain and the drug loaded peptide hydrogel suggesting that drug encapsulation did not affect ac-$(RADA)_4$-$CONH_2$ rigidity.

DOX and CUR release from ac-$(RADA)_4$-$CONH_2$ peptide nanofiber hydrogel

The *in vitro* release profiles of DOX and CUR from ac-$(RADA)_4$-$CONH_2$ peptide hydrogel were monitored in PBS pH 7.4. An initial burst release from the peptide hydrogel for the more hydrophilic DOX (logP: 1.27) (*ca*. 73 %) was observed in PBS pH 7.4 within less than 4 h, while total drug release was achieved within 4 days (Figure 3A). At the same time scale of 4 h, the hydrophobic CUR (logP: 3.29) release reached only 49 % of its total content in the peptide hydrogel, showing a slower release rate compared to DOX, followed by a sustained release over 20 days (Figure 3B). The burst release effect could be attributed to the actives release from the

exposed top layer of the hydrogel upon contact with the release medium. The sustained release of hydrophobic molecules from other self-assembling peptide hydrogel systems has been previously reported and associated to the interactions between the solute molecules and the hydrophobic functionalities of the peptide nanofibers (19,20,34,35). Li I-C. et al. (2016) demonstrated that intrafibrillar drug encapsulation in multidomain peptide nanofibers of various small molecule drugs with poor water solubility resulted in prolonged drug release profiles (36). In the present study, the ac-$(RADA)_4$-$CONH_2$ peptide hydrogel was found to control release based on drug hydrophobicity, suggesting that it may be an efficient drug delivery depot system for topical administration.

DOX and CUR release kinetics from the ac-$(RADA)_4$-$CONH_2$ peptide nanofiber hydrogel

The release profiles of both CUR and DOX from the ac-$(RADA)_4$-$CONH_2$ peptide hydrogel were found to best fit the Korsmeyer-Peppas kinetic model (R^2=0.971 and 0.973, respectively). The exponent of n obtained values for DOX and CUR of 0.393 and 0.417, respectively, indicating a Fickian diffusion mechanism of drug release from the hydrogel matrix ($n<0.45$), whereas the K_H values were 9.14 and 5.79, respectively.

Localization of the fluorescent actives CUR and DOX within the ac-$(RADA)_4$-$CONH_2$ peptide nanofiber hydrogel

The distribution of the fluorescent CUR and DOX within the peptide nanofiber hydrogel was visualized by CLSM. A stronger green fluorescence, compared to the surrounding aqueous background, delineated the peptide nanofiber suggesting a close interaction of the hydrophobic CUR with the hydrophobic domains of the peptide nanofibers (Figure 4A) (34). On the other

hand, the scattered red fluorescent signal of the more hydrophilic DOX (Figure 4B) suggests a homogeneous distribution of the drug molecules in the aqueous environment of the peptide hydrogel. The distinctive localization of each type of drug molecule within the peptide carrier further corroborates the results obtained from the *in vitro* release studies, where the favorable interaction of the hydrophobic CUR with the peptide nanofibers results in a slower release pattern over time, whereas a faster release profile was observed for the more hydrophilic DOX.

***In vitro* cytotoxicity study**

The half maximal inhibitory concentration values (IC_{50}) of CUR and DOX were evaluated after cell treatment for 48 h and were found to be 5.76 μM ($\pm$ $1.28 \cdot 10^{-6}$) and 0.682 μM ($\pm$ $0.578 \cdot 10^{-7}$), respectively. The *in vitro* anti-proliferative effect of the drug loaded ac-$(RADA)_4$-$CONH_2$ peptide hydrogel compared to the plain drug solutions was investigated by the MTT assay. All treatments induced a growth inhibitory effect on U-87 MG cells in a dose-dependent manner. DOX inhibited U-87 MG cell growth much more considerably when loaded within the peptide hydrogel for concentrations below the IC_{50} of the drug, compared to the plain drug solution (Figure 5B), denoting the effectiveness of the system at lower drug doses. On the contrary, a higher cytotoxic effect was observed for the plain CUR solution compared to its hydrogel loaded congener (Figure 5A). This effect might be attributed to the slower rate of CUR release from the peptide hydrogel, such that cells are exposed to lower drug concentrations when treated with the peptide hydrogel formulation. These observations are in good agreement with previous studies where CUR cytotoxicity has been related with the rate of drug release from the carrier (37). The peptide nanofiber hydrogel was shown to be not cytotoxic against U-87 MG cells, suggesting that the cytotoxic effect that we observed in the case of the DOX and CUR peptide hydrogel

formulations is not due to the peptide hydrogel. The biocompatibility of the ac-$(RADA)_4$-$CONH_2$ hydrogel has already been validated in numerous biomedical (38-40) and drug delivery applications (41-43).

DOX and CUR internalization studies in U-87 MG cells

CLSM studies

The intracellular distribution of DOX and CUR in U-87 MG cells was investigated time-dependently by CLSM after cell exposure to the plain drug solutions and the drug loaded peptide hydrogel in concentrations corresponding to their IC_{50} values.

DOX is known to exert its anti-tumor activity through DNA intercalation (28). DOX exhibited a targeted accumulation inside cell nuclei independently of the dosage form, even at the earliest stages of drug treatment (Figure 6A). Higher levels of DOX uptake were observed in ac-$(RADA)_4$-$CONH_2$-DOX treated cells, as indicated by the stronger red fluorescence of cell nuclei, also accompanied by a significant compromise in nuclear DAPI staining (44). This is clearly exemplified after 6 h of treatment with ac-$(RADA)_4$-$CONH_2$-DOX, where almost no DAPI fluorescence of cell nuclei was acquired. It can be therefore concluded that ac-$(RADA)_4$-$CONH_2$ -DOX formulation effectively enhanced DOX cellular uptake and nuclear accumulation, compared to the plain drug solution.

CUR uptake by U-87 MG cells after treatment with the plain drug solution or the CUR loaded peptide hydrogel is depicted in Figure 6B. Cells exposed to CUR solution demonstrated an intense green fluorescence evenly distributed both in the cytoplasm and nucleus, which was retained throughout the 1.5 h treatment. A significant decrease in fluorescence intensity was observed thereafter, resulting in signal disappearance after the 6 h treatment with CUR solution.

Comparable results have been previously reported by Kunwar et al. (45) and Sun et al. (46), that monitored a maximum CUR uptake at the initial stages of drug treatment (2-3 h), accompanied by a subsequent decrease of CUR uptake as a function of time. A gradual and moderate increase in cellular accumulation of CUR from the peptide hydrogel formulation was evidenced at the initial stages of cell treatment, followed by a substantial decrease in cell fluorescence after the 3 hours of cell exposure. Cells treated with the peptide hydrogel formulation are exposed to lower CUR levels, since drug diffusion from the peptide hydrogel is the rate limiting factor for cellular uptake. This could partly define the different gradient observed in CUR cellular accumulation between the plain drug solution and the drug loaded peptide hydrogel.

Flow cytometric analysis

Flow cytometry was employed to further quantitatively confirm intracellular accumulation of CUR and DOX in U-87 MG cells. Histogram profiles of DOX cellular uptake are shown in Figure 7A. DOX fluorescence intensity of the cells treated with both the plain drug solution and the drug loaded peptide hydrogel demonstrated a progressive increase, indicating a continuous drug uptake process. In accordance with the qualitative assessment of DOX uptake by confocal microscopy, a profoundly higher DOX accumulation was observed in cells treated with the ac-$(RADA)_4$-$CONH_2$-DOX formulation, compared to those treated with the plain drug solution. The difference remained statistically significant at all time-points evaluated (0.5 - 6 h), designating the superiority of the peptide hydrogel carrier for DOX delivery.

The cellular uptake efficiency of CUR loaded ac-$(RADA)_4$-$CONH_2$ peptide hydrogel was poor, as evident by flow cytometric analysis (Figure 7B). Fluorescence intensity of the cells treated with the ac-$(RADA)_4$-$CONH_2$-CUR formulation was comparable to the auto-fluorescent signal

of untreated cells, with only a slight increase in cellular CUR accumulation observed after 3 h of treatment. The cellular uptake profile of CUR solution by U-87 MG cells was determined to be more effective when CUR was released from ac-$(RADA)_4$-$CONH_2$-CUR formulation, also showing a time-dependent decrease of intracellular drug accumulation after the third hour of treatment.

Apoptotic efficacy of ac-$(RADA)_4$-$CONH_2$-CUR peptide hydrogel

Cell apoptosis was evaluated by flow cytometry using the Annexin-V-FITC/PI double staining, after cell treatment with the plain CUR solution and the drug loaded peptide hydrogels (Figure 8). Compared to untreated cells, drug exposure induced a higher apoptotic effect on U-87 MG cells after treatment for 48 h. Interestingly, the percentage of early apoptotic cells was enhanced upon CUR loading within the peptide hydrogel, compared to the respective plain drug solution (t-test, $p<0.05$).

Conclusions

In the present study, we demonstrated the feasibility of an in-situ gel forming self-assembling peptide hydrogel, ac-$(RADA)_4$-$CONH_2$, to encapsulate and release chemotherapeutic drug molecules of both high and low aqueous solubility against U-87 MG cancer cell line. Drug encapsulation within the ac-$(RADA)_4$-$CONH_2$ did not affect the rheological properties of the peptide hydrogel. The water insoluble CUR demonstrated strong interaction with the peptide nanofibers resulting in nanofiber localization of CUR which in turn resulted in a sustained drug release profile over 20 days. On the other hand, the water soluble DOX showed a homogeneous distribution in the aqueous environment of the peptide hydrogel resulting in a burst release

profile and in complete drug release within 4 days. A higher DOX intracellular accumulation and a higher antiproliferative effect on U-87 MG cells was observed after treatment with the ac-$(RADA)_4$-$CONH_2$-DOX formulation, compared to DOX solution. CUR cellular uptake and antiproliferative efficacy on U-87 MG cells treated with ac-$(RADA)_4$-$CONH_2$-CUR was less pronounced, attributed to the more sustained drug release from the peptide hydrogel. Overall, the results demonstrate that the ac-$(RADA)_4$-$CONH_2$ peptide hydrogel system merits further investigation as an in-situ gel forming depot system for the efficient delivery of both water-soluble and poorly water-soluble chemotherapeutic agents in the local treatment of cancer.

Corresponding Author

Dr Dimitrios G. Fatouros, e-mail: dfatouro@pharm.auth.gr

Author Contributions

The manuscript was written through contributions of all authors. All authors have given approval to the final version of the manuscript.

Acknowledgments

C.K. is supported by the Onassis Foundation with a PhD scholarship. We thank Orestis L. Katsamenis from μ-VIS X-ray Imaging Centre, Faculty of Engineering and the Environment, University of Southampton, Southampton for the SEM studies. We would like to thank Dr. A. Lazaridou from Department of Food Science and Technology, School of Agriculture, Aristotle University of Thessaloniki, Greece for her assistance in the rheology measurements.

Conflict of Interest

The authors declare that they have no conflict of interest.

References

1. Bastiancich C, Danhier P, Préat V, Danhier F. Anticancer drug-loaded hydrogels as drug delivery systems for the local treatment of glioblastoma. J Control Release. 2016;243:29-42.
2. Stupp R, Brada M, van den Bent MJ, Tonn JC, Pentheroudakis G. High-grade glioma: ESMO clinical practice guidelines for diagnosis, treatment and follow-up. Ann Oncol 2014;25:93-101.
3. Patel DM, Agarwal N, Tomei KL, Hansberry DR, Goldstein IM. Optimal timing of whole-brain radiation therapy following craniotomy for cerebral malignancies. World Neurosurg. 2015;84(2):412-419.
4. Hervey-Jumper SL, Berger MS. Maximizing safe resection of low- and high-grade glioma. J Neurooncol. 2016;130(2):269-282.
5. Holland EC. Glioblastoma multiforme: the terminator. Proc Natl Acad Sci USA. 2000; 97(12): 6242-6244.
6. Jelsma R, Bucy PC. The treatment of glioblastoma multiforme of the brain. J Neurosurg. 1967;27(5):388-400.
7. Reardon DA, Wucherpfennig KW, Freeman G, Chiocca EA, Wen PY, Curry WT, Jr Mitchell A, Fecci P, Sampson JH. An update of vaccine therapy and other immunotherapeutic approaches for glioblastoma. Expert Rev Vaccines. 2014;12(6):597-615.
8. Karim R, Palazzo C, Evrard B, Piel G. Nanocarriers for the treatment of glioblastoma multiforme: current state-of-the-art. J Control Release. 2016;227:23-37.
9. Wolinsky JB, Colson YL. Local drug delivery strategies for cancer treatment: gels, nanoparticles, polymeric films, rods and wafers. J Control Release. 2012;159(1):14-26.
10. Chakroun RW, Zhang P, Lin R, Schiapparelli P, Quinones-Hinojosa A, Cui H.

Nanotherapeutic systems for local treatment of brain tumors. Wiley Interdiscip Rev Nanomed Nanobiotechnol. 2017;10(1) doi: 10.1002/wnan.1479.

11. Tian R, Chen J, Niu R. The development of low-molecular weight hydrogels for applications in cancer therapy. Nanoscale. 2014;6(7):3474-3482.
12. Yu L, Ding J. Injectable hydrogels as unique biomedical materials. Chem Soc Rev. 2008;37(8): 1473-1481.
13. Fourniols T, Randolph LD, Staub A, Vanvarenberg K, Leprince JG, Préat V, Des Rieux A, Danhier F. Temozolomide-loaded photopolymerizable PEG-DMA-based hydrogel for the treatment of glioblastoma. J Control Release. 2015;210:95-104.
14. Bastiancich C, Vanvarenberg K, Ucakar B, Pitorre M, Bastiat G, Lagarce F, Préat V, Danhier F. Lauroyl-gemcitabine-loaded lipid nanocapsule hydrogel for the treatment of glioblastoma. J Control Release. 2016;225:283-293.
15. Tauro JR, Gemeinhart RA. Matrix metalloproteinase triggered delivery of cancer chemotherapy from hydrogel matrixes. Bioconjug Chem. 2005;16(5):1133-1139.
16. Meenach SA, Shapiro JM, Hilt JZ, Anderson KW. Characterization of PEG-iron oxide hydrogel nanocomposites for dual hyperthermia and paclitaxel delivery. J Biomater Sci Polym. 2013;24(9):1112-1126.
17. Tsao CT, Kievit FM, Ravanpay A, Erickson AE, Jensen MC, Ellenbogen RG, Zhang M. Thermoreversible poly(ethylene glycol)-g-chitosan hydrogel as a therapeutic T lymphocyte depot for localized glioblastoma immunotherapy. Biomacromolecules. 2014;15(7):2656-2662.
18. Jain A, Betancur M, Patel GD, Valmikinathan CM, Mukhatyar VJ, Vakharia A, Pai SB, Brahma B, MacDonald TJ, Bellamkonda RV. Guiding intracortical brain tumour cells to an

extracortical cytotoxic hydrogel using aligned polymeric nanofibres. Nat Mater. 2014;13(3):308-316.

19. Koutsopoulos S, Unsworth LD, Nagai Y, Zhang SG. Controlled release of functional proteins through designer self-assembling peptide nanofiber hydrogel scaffold. Proc Natl Acad Sci USA. 2009;106(12):4623-4628.
20. Nagai Y, Unsworth LD, Koutsopoulos S, Zhang S. Slow release of molecules in self-assembling peptide nanofiber scaffold. J Control Release. 2006;115(1):18-25.
21. Thota CK, Yadav N, Chauhan VS. A novel highly stable and injectable hydrogel based on a conformationally restricted ultrashort peptide. Scientific Reports. 2016;6:31167.
22. Li X, Fu M, Wu J, Zhang CY, Deng X, Dhinakar A, Huang WL, Qian, Ge L. pH-sensitive peptide hydrogel for glucose-responsive insulin delivery. Acta Biomaterialia. 2017;51:294-303.
23. Kopesky PW, Byun S, Vanderploeg EJ, Kisiday JD, Frisbie DD, Grodzinsky AJ. Sustained delivery of bioactive TGF-beta 1 from self-assembling peptide hydrogels induces chondrogenesis of encapsulated bone marrow stromal cells. J Biomed Mater Res A. 2014;102(5):1275-1285.
24. Liebesny PH, Byun S, Hung HH, Pancoast JR, Mroszczyk KA, Young WT, Lee RT, Frisbie DD, Kisiday JD, Grodzinsky AJ. Growth Factor-Mediated Migration of Bone Marrow Progenitor Cells for Accelerated Scaffold Recruitment. Tissue Engineering Part A. 2016;22(13-14): 917-927.
25. Koutsopoulos S. Self-assembling peptide nanofiber hydrogels in tissue engineering and regenerative medicine: Progress, design guidelines, and applications. J Biomed Mater Res A. 2016;104(4):1002–1016.

26. Acar H, Srivastava S, Chung EJ, Schnorenberg MR, Barrett JC, LaBelle JL, Tirrell M. Self-assembling peptide-based building blocks in medical applications. Adv Drug Deliv Rev. 2017;110-111:65-79.
27. Cormier AR, Pang X, immerman MI, Zhou HX, Paravastu AK. Molecular structure of RADA16-I designer self-assembling peptide nanofibers. ACS Nano. 2013;7:7562-7572.
28. Momparler RL, Karon M, Siegel SE, Avila F. Effect of adriamycin on DNA, RNA, and protein synthesis in cell-free systems and intact cells. Cancer Res. 1976;36:2891-2895.
29. Sordillo, LA, Sordillo PP, Helson L. Curcumin for the Treatment of Glioblastoma. Anticancer Res. 2015;35(8):6373-6378.
30. Cajot S, Van Butsele K, Paillard A, Passirani C, Garcion E, Benoit JP, Varshney SK, Jérôme C. Smart nanocarriers for pH-triggered targeting and release of hydrophobic drugs. Acta Biomater. 2012;8(12):4215-4223.
31. Manchun S, Dass CR, Sriamornsak P. Targeted therapy for cancer using pH-responsive nanocarrier systems. Life Sci. 2012;90(11-12):381-387.
32. Ritger PL, Peppas NA. A simple equation for description of solute release ii. fickian and anomalous release from swellable devices. J Control Release. 1987;5(1):37-42.
33. Zhang Y, Huo M, Zhou J, Zou A, Li W, Yao C, Xie S. DDSolver: an add-in program for modeling and comparison of drug dissolution profiles. AAPS J. 2010;12(3):263-271.
34. Altunbas A, Lee SJ, Rajasekaran SA, Schneider JP, Pochan DJ. Encapsulation of curcumin in self-assembling peptide hydrogels as injectable drug delivery vehicles. Biomaterials. 2011;32(25):5906-5914.
35. Liu J, Zhang L, Yang Z, Zhao X. Controlled release of paclitaxel from a self-assembling peptide hydrogel formed in situ and antitumor study in vitro. Int J Nanomedicine.

2011;6:2143-2153.

36. Li I-C, Moore AN, Hartgerink JD. “Missing Tooth” Multidomain Peptide Nanofibers for Delivery of Small Molecule Drugs. Biomacromolecules. 2016;17:2087–2095
37. Liu J, Liu J, Xu H, Zhang Y, Chu L, Liu Q, Song N. Novel tumor-targeting, self-assembling peptide nanofiber as a carrier for effective curcumin delivery. Int J Nanomedicine. 2014;9:197-207.
38. Koutsopoulos S, Zhang S. Long-term three-dimensional neural tissue cultures in functionalized self-assembling peptide hydrogels, Matrigel and Collagen I. Acta Biomater 2013;9(2):5162-5169.
39. Cheng TY, Chen MH, Chang WH, Huang MY, Wang TW. Neural stem cells encapsulated in a functionalized self-assembling peptide hydrogel for brain tissue engineering. Biomaterials. 2013;34(8):2005-2016.
40. Wang X, Wang J, Guo L, Wang X, Chen H, Wang X, Liu J, Tredget EE, Wu Y. Self-assembling peptide hydrogel scaffolds support stem cell-based hair follicle regeneration. Nanomedicine Nanotechnology Biol Med. 2016;12(7):2115-2125.
41. Koutsopoulos S, Zhang S. Two-layered injectable self-assembling peptide scaffold hydrogels for long-term sustained release of human antibodies. J Control Release. 2012;160(3):451-458.
42. Zhou A, Chen S, He B, Zhao W, Chen X. Controlled release of TGF-beta 1 from RADA self-assembling peptide hydrogel scaffolds. Drug Des Devel Ther. 2016;10:3043-3051.
43. Karavasili C, Komnenou A, Katsamenis OL, Charalampidou G, Kofidou E, Andreadis D, Koutsopoulos S, Fatouros DG. Self-assembling peptide nanofiber hydrogels for controlled ocular delivery of timolol maleate. ACS Biomater Sci Eng. 2017;3(12):3386-3394.

44. Brosseau N, Andreev E, Ramotar D. Complementation of the yeast model system reveals that caenorhabditis elegans OCT-1 Is a functional transporter of anthracyclines. PLoS One. 2015;10 (7):e0133182.
45. Kunwar A, Barik A, Mishra B, Rathinasamy K, Pandey R, Priyadarsini KI. Quantitative cellular uptake, localization and cytotoxicity of curcumin in normal and tumor cells. Biochim Biophys Acta - Gen Subj. 2008;1780(4):673-679.
46. Sun J, Bi C, Chan HM, Sun S, Zhang Q, Zheng Y. Curcumin-loaded solid lipid nanoparticles have prolonged in vitro antitumour activity, cellular uptake and improved in vivo bioavailability. Colloids Surf B Biointerfaces. 2013;111:367-375.

Legends to Figures

FIGURE 1: Scanning electron micrograph of ac-$(RADA)_4$-$CONH_2$ peptide nanofiber hydrogel.

FIGURE 2: Mechanical properties of the empty and drug loaded peptide hydrogel. **A**. Time dependence of storage (G') and loss (G'') moduli of ac-$(RADA)_4$-$CONH_2$ peptide nanofiber hydrogels (1 Hz, 0.5 % strain, 37 °C) and **B**. Frequency dependence of G′ and G″ of the formed peptide nanofiber hydrogels (strain 0.5 %, 37 °C).

FIGURE 3: *In vitro* release profiles of **A.** DOX and **B.** CUR from the ac-$(RADA)_4$-$CONH_2$ peptide hydrogel in PBS pH 7.4 at 37 ^oC. Results are presented as means ± S.D. (n=3).

FIGURE 4: CLSM (63x objective) z-stack images of ac-$(RADA)_4$-$CONH_2$ peptide hydrogel loaded with the fluorescent actives **A**. CUR and **B**. DOX. Scale bar: 10 μm.

FIGURE 5: Cell viability of U-87 MG cells as determined by the MTT assay after treatment with different concentrations of free and ac-$(RADA)_4$-$CONH_2$ peptide hydrogel loaded with **A.** CUR and **B.** DOX for 48 h. Results are presented as means ± S.D. (n=3).

FIGURE 6: CLSM images of U-87 MG cells after treatment with **A.** DOX solution and ac-$(RADA)_4$-$CONH_2$-DOX (0.682 μM) and **B.** CUR solution and ac-$(RADA)_4$-$CONH_2$-CUR (5.86 μM) for 0.5 h, 1.5 h, 3 h and 6 h. Blue fluorescence corresponds to DAPI stained cell nuclei, red to DOX and green to CUR fluorescence. Scale bar: 20 μm.

FIGURE 7: Flow cytometry histograms (left panel) and mean fluorescence intensity (right panel) of U-87 MG cell uptake after treatment with **A.** DOX solution and ac-$(RADA)_4$-$CONH_2$-DOX (0.682 μM) and **B.** CUR solution and ac-$(RADA)_4$-$CONH_2$-CUR (5.86 μM) for 0.5 h, 1.5 h, 3 h and 6 h. Fluorescence intensities are presented as means ± S.D. (n=3, $^{*}p < 0.05$).

FIGURE 8: Cell apoptosis analysis in U-87 MG cells determined with flow cytometry by double staining with Annexin-V-FITC and PI after treatment with CUR solution or ac-$(RADA)_4$-$CONH_2$-CUR for 48 h. **A.** Data show the distribution of cells with necrosis in quadrant 1 (Q1), late apoptosis in quadrant 2 (Q2), viable cells in quadrant 3 (Q3) and early apoptosis in quadrant 4 (Q4). **B.** The percentages plotted indicate the percentage of Annexin-V-FITC/PI positive (late apoptotic) and Annexin-V-FITC positive (early apoptotic) cells. The data are representative of three independent experiments ± S.D.

FIGURE 1

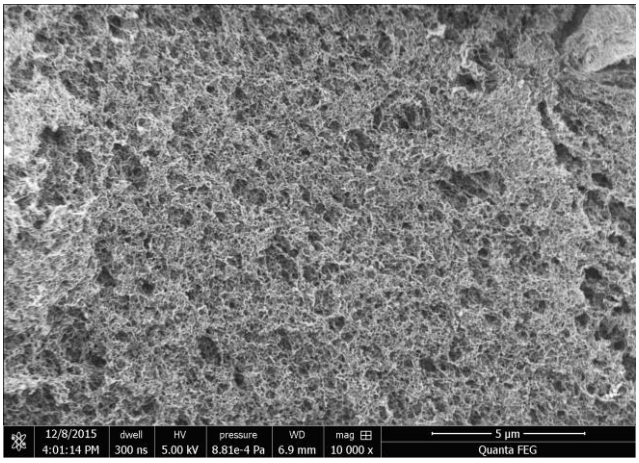
12/8/2015
4:01:14 PM
dwell
300 ns
HV
5.00 kV
pressure
8.81e-4 Pa
WD
6.9 mm
mag
10 000 x
5 µm
Quanta FEG

FIGURE 2

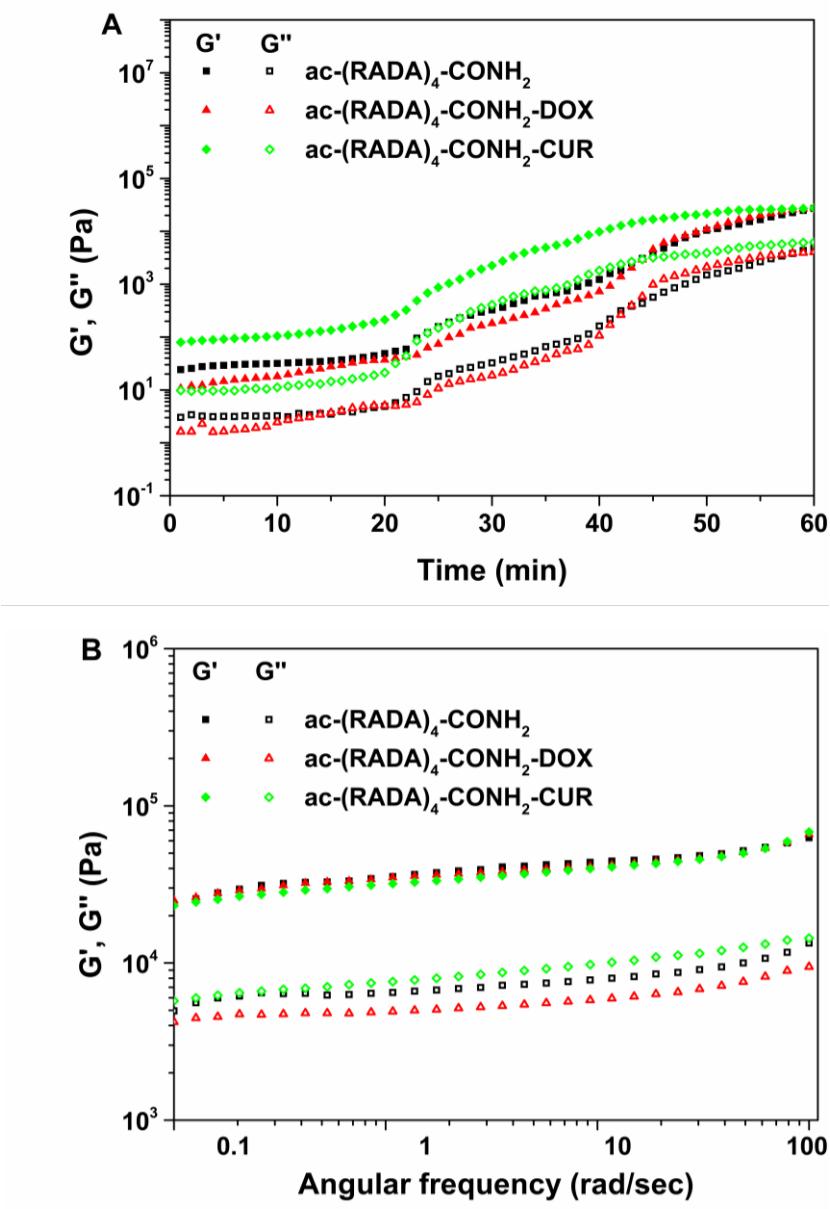
A
G'
G''
ac-(RADA)4-CONH2
ac-(RADA)4-CONH2-DOX
ac-(RADA)4-CONH2-CUR
G', G'' (Pa)
Time (min)
B
G'
G''
ac-(RADA)4-CONH2
ac-(RADA)4-CONH2-DOX
ac-(RADA)4-CONH2-CUR
G', G'' (Pa)
Angular frequency (rad/sec)

FIGURE 3

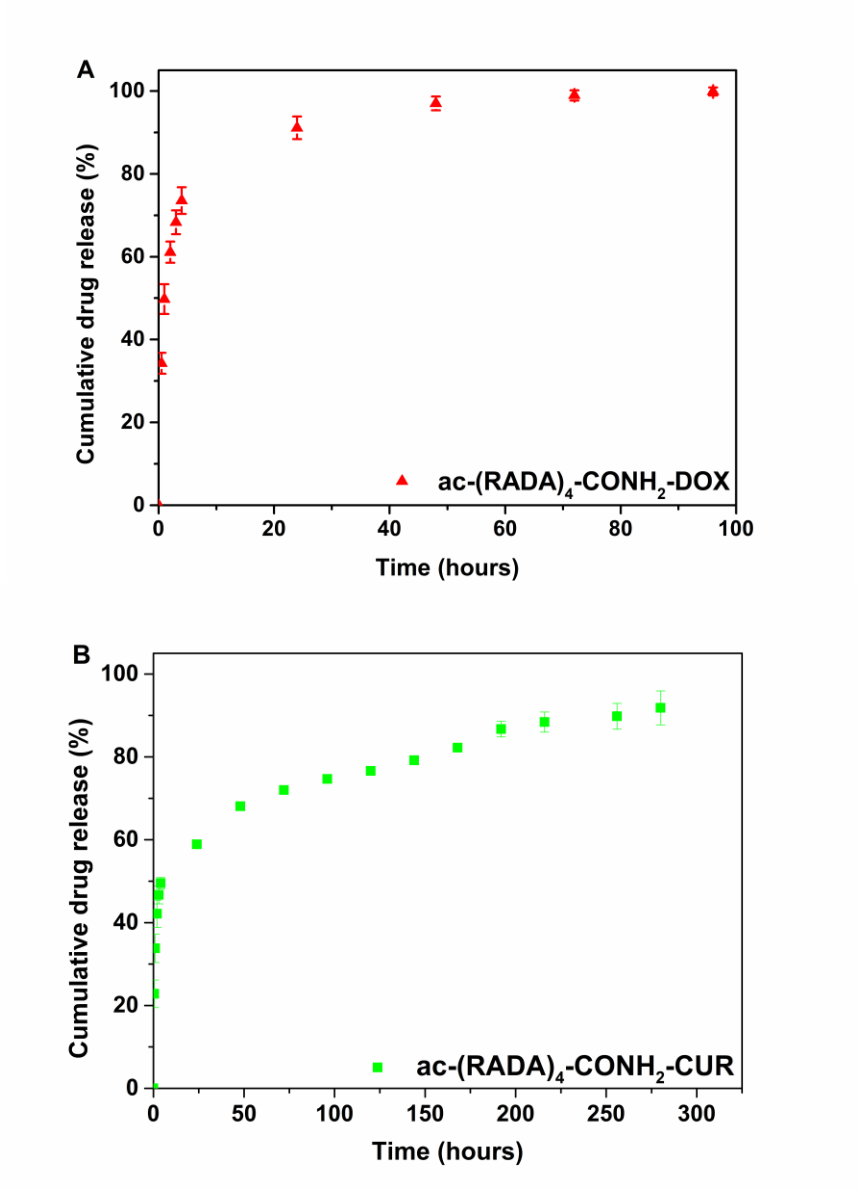
A
Cumulative drug release (%)
Time (hours)
ac-(RADA)4-CONH2-DOX
B
Cumulative drug release (%)
Time (hours)
ac-(RADA)4-CONH2-CUR

FIGURE 4

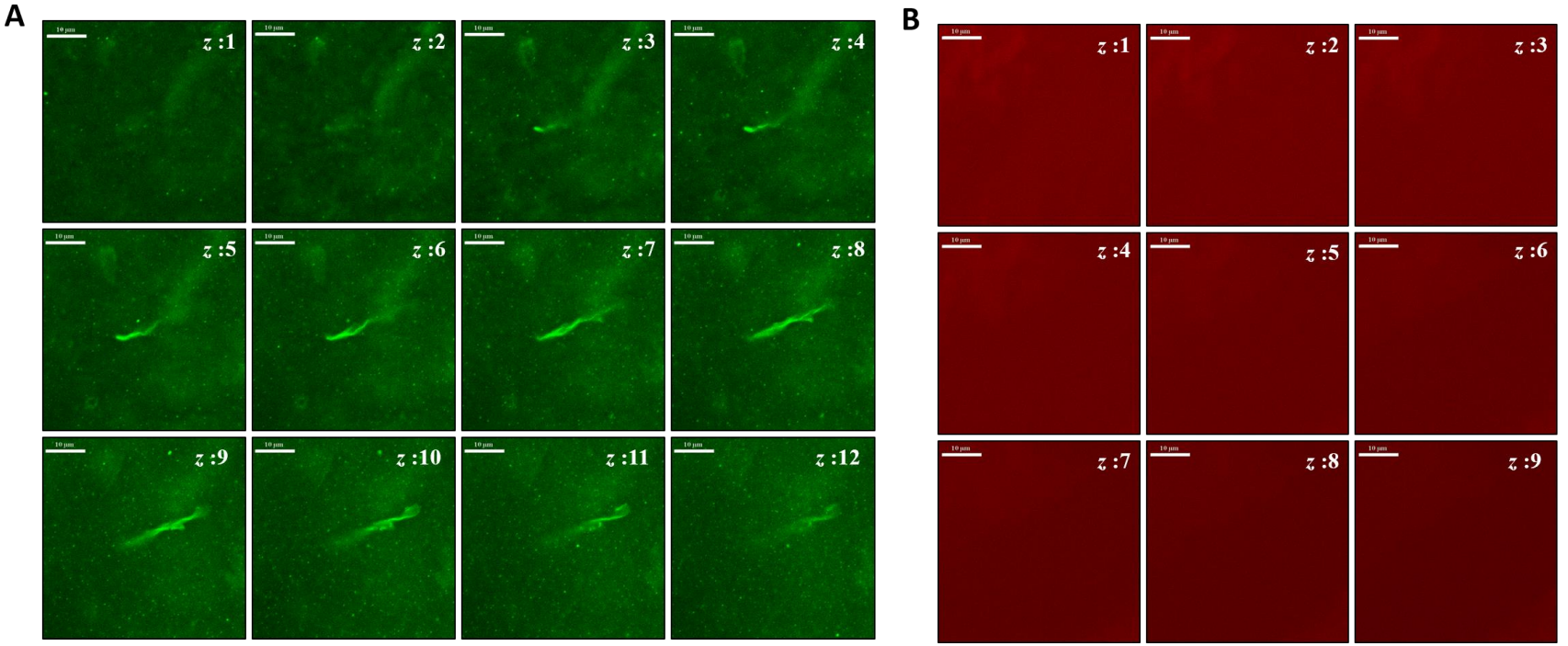

FIGURE 5

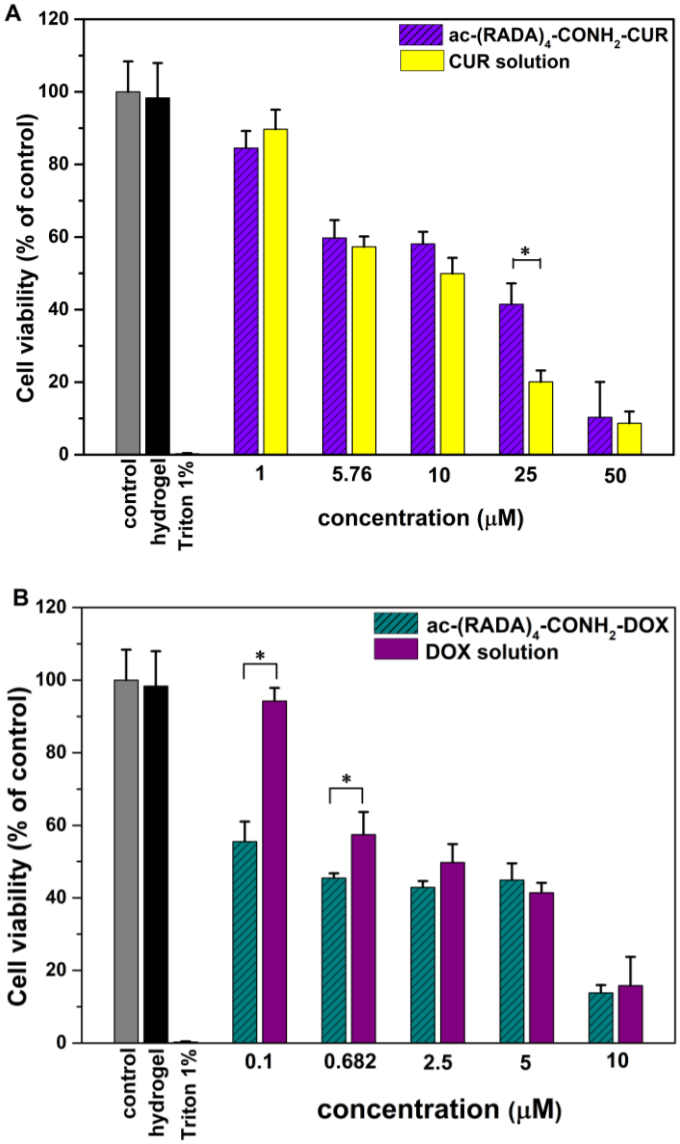
A
ac-(RADA)4-CONH2-CUR
CUR solution
Cell viability (% of control)
120
100
80
60
40
20
0
control
hydrogel
Triton 1%
1
5.76
10
25
50
concentration (μM)
*
B
ac-(RADA)4-CONH2-DOX
DOX solution
Cell viability (% of control)
120
100
80
60
40
20
0
control
hydrogel
Triton 1%
0.1
0.682
2.5
5
10
concentration (μM)
*
*

FIGURE 6

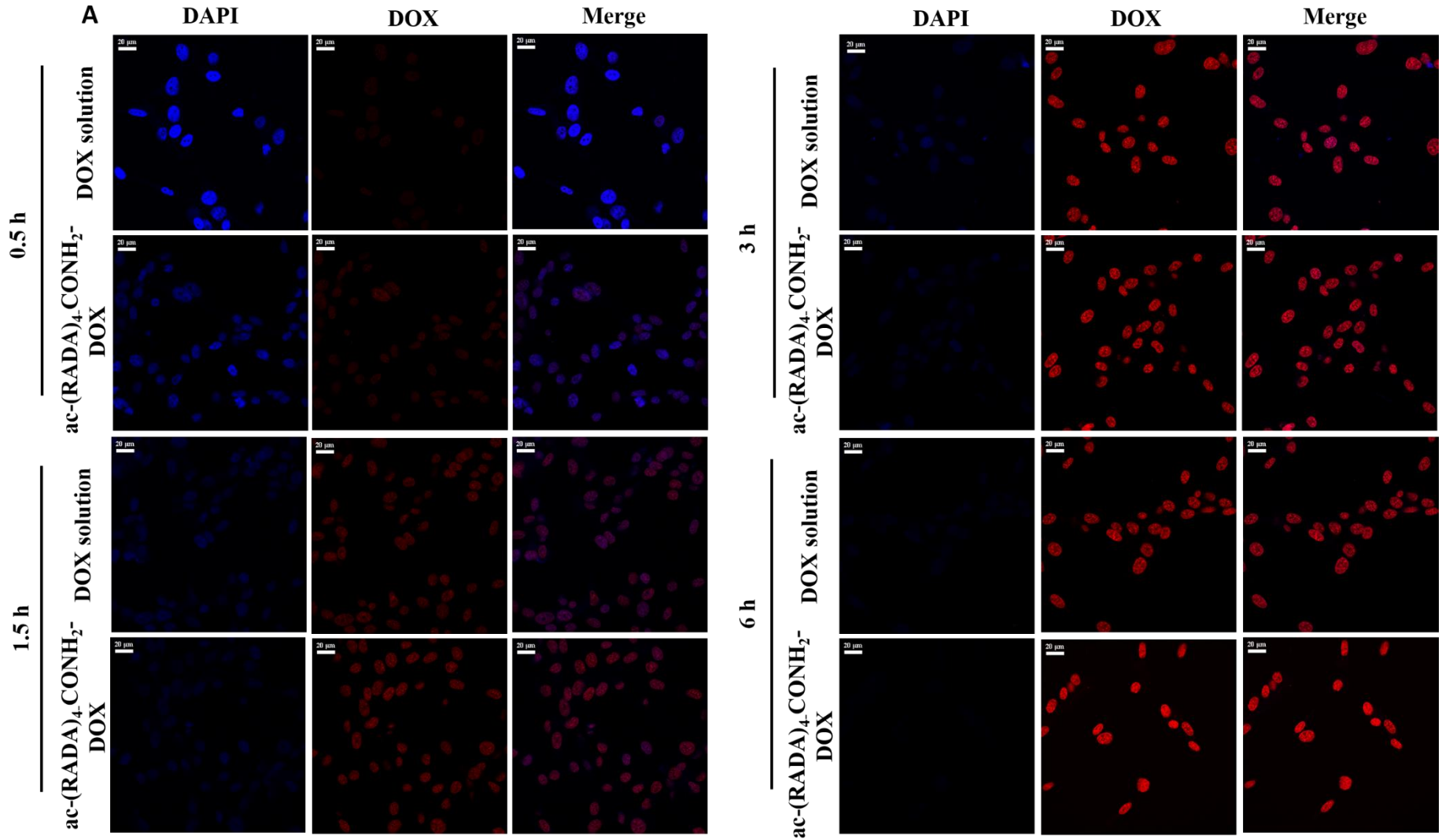
A
DAPI
DOX
Merge
0.5 h
1.5 h
3 h
6 h
DOX solution
ac-(RADA)4-CONH2-DOX
20 μm

B
DAPI
CUR
Merge
0.5 h
1.5 h
3 h
6 h
CUR solution
ac-(RADA)4CONH2-CUR
20 μm

FIGURE 7

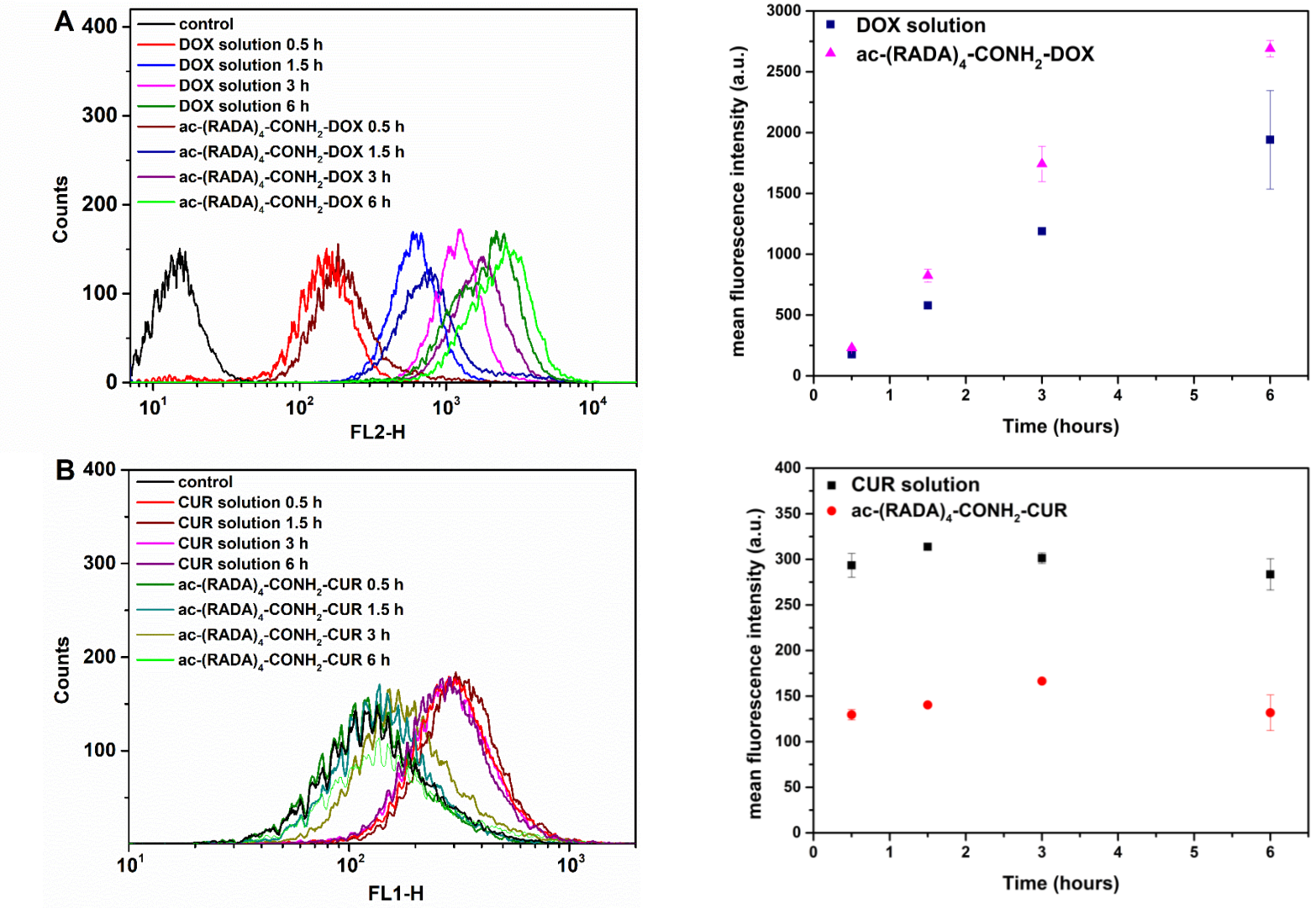
A
control
DOX solution 0.5 h
DOX solution 1.5 h
DOX solution 3 h
DOX solution 6 h
ac-(RADA)4-CONH2-DOX 0.5 h
ac-(RADA)4-CONH2-DOX 1.5 h
ac-(RADA)4-CONH2-DOX 3 h
ac-(RADA)4-CONH2-DOX 6 h
Counts
FL2-H
B
control
CUR solution 0.5 h
CUR solution 1.5 h
CUR solution 3 h
CUR solution 6 h
ac-(RADA)4-CONH2-CUR 0.5 h
ac-(RADA)4-CONH2-CUR 1.5 h
ac-(RADA)4-CONH2-CUR 3 h
ac-(RADA)4-CONH2-CUR 6 h
Counts
FL1-H
DOX solution
ac-(RADA)4-CONH2-DOX
mean fluorescence intensity (a.u.)
Time (hours)
CUR solution
ac-(RADA)4-CONH2-CUR
mean fluorescence intensity (a.u.)
Time (hours)

FIGURE 8

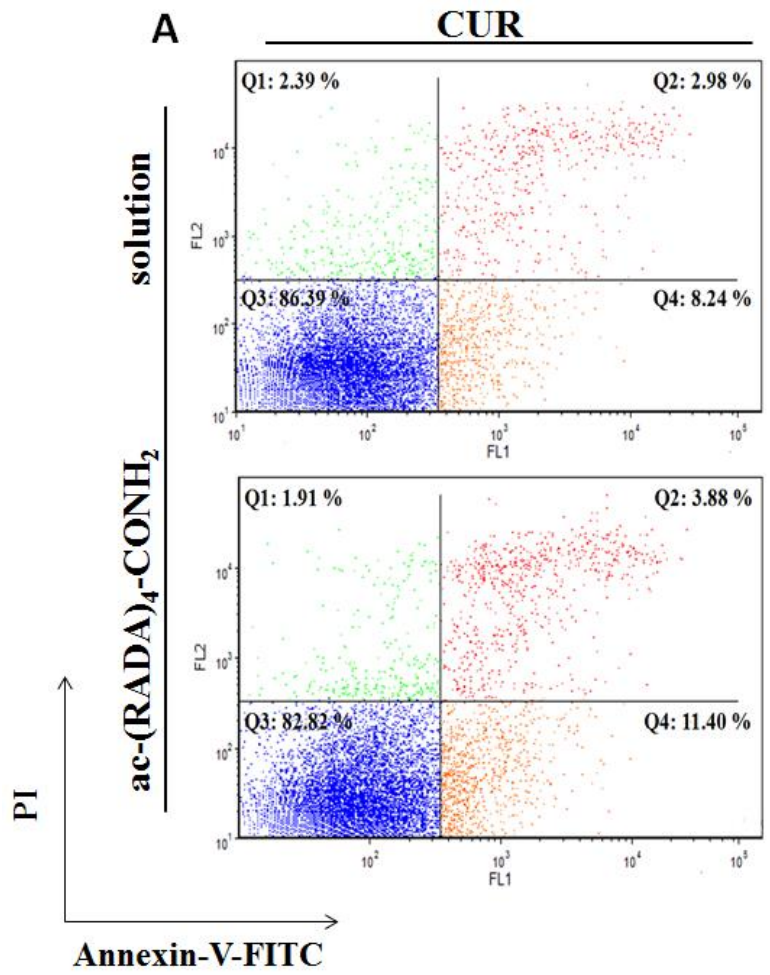
A
CUR
solution
ac-(RADA)4-CONH2
Q1: 2.39 %
Q2: 2.98 %
Q3: 86.39 %
Q4: 8.24 %
Q1: 1.91 %
Q2: 3.88 %
Q3: 82.82 %
Q4: 11.40 %
FL1
FL2
PI
Annexin-V-FITC
B
late apoptosis
early apoptosis
CUR solution
ac-(RADA)4-CONH2- CUR
% apoptosis
control
curcumin